

## Chapter 3

### Warming-induced experimental epidemics are predicted by metabolic theory but not early warning signals

#### Abstract

Environmental conditions can mediate the spread of infectious disease, but the mechanisms by which climate warming causes disease emergence remain poorly understood and our ability to predict disease emergence remains limited. We developed a predictive framework for the thermal dependence of epidemics by merging the metabolic theory of ecology (MTE) with classical epidemiological theory and tested the resulting model using disease incidence data from populations of an experimental host-parasite system held under slowly warming versus constant environmental conditions. In agreement with independently obtained model predictions, epidemics established in our experimental *Daphnia* – microsporidian populations once temperatures surpassed 11.5°C. In contrast, the experimental data and model simulations revealed no clear evidence of early warning signals for the temperature-induced critical transition of the host-parasite system into an epidemic state. Our study serves as a proof of principle that applying the MTE framework to host-parasite systems can provide a valuable tool for predicting the effects of both climatic and seasonal warming on infectious disease epidemics.

\*Authorship note: a version of this manuscript is under submission as the following reference:

Kirk D°, Luijckx P°, Jones N, Krichel L, Pencer C, Molnár P, Krkosek M. Warming-induced experimental epidemics are predicted by metabolic theory but not early warning signals. Submitted. ° Represents equal author contributions.

## Main Text

Despite the ecological and economic impacts of infectious disease epidemics in human (Lee et al. 2013, Hotez et al. 2014), agricultural (Chakraborty & Newton 2011), and wildlife populations (Krkosek et al. 2006), our current ability to understand and predict how epidemics emerge or are altered by climate change is complicated by temperature's various simultaneous effects on a system. The emergence, severity, and duration of epidemics depend on the characteristics of the host-parasite system in question, such as host density (Lloyd-Smith et al. 2005), the ability of a parasite to infect its host (Duffy & Sivars-Becker 2007), and the balance between transmission and host exploitation that underlies virulence (Galvani 2003). These key parameters often vary with the external environment. Because of the direct link between temperature and host-parasite dynamics in many systems, temperature changes associated with seasonality and climate change can also underlie disease emergence and the severity of epidemics (Marcogliese 2008). Two distinct areas of ecological theory hold promise as frameworks for predicting disease emergence due to climate warming – the metabolic theory of ecology and the theory of early warning signals of critical transitions - but experimental tests of these theories to predict disease are lacking.

Studies using observational time series have linked warming temperatures or temperature variability to increased disease and die-offs, including in sea stars (Harvell et al 2019), frogs (Pounds et al. 2006), and human malaria (Zhou et al. 2004). One mechanistic basis for disease-climate links lies in the thermal dependence of disease traits, including virulence (Paull et al. 2012), contact rate (Kirk et al. 2019), and within-host parasite growth (Kirk et al. 2018). However, observational studies are necessarily confounded by uncontrollable and, in some cases,

unidentified variables that co-vary with environmental conditions. For example, Rohr and colleagues (2008) found that evidence for the purported causal link between temperature and frog die-offs was weak, and that other non-climatic variables were better predictors of extinction than temperature. A key problem is that various traits determining the course of epidemics can differ in the strength and direction of their respective temperature dependencies (Mordecai et al. 2013, Mordecai et al. 2017, Shapiro et al. 2017). Thus, to understand and predict the net effect of warming on epidemics we need to combine thermal dependencies with mechanistic models of disease spread (e.g. Mangal et al. 2008, Mordecai et al. 2013, Mordecai et al. 2017, Shapiro et al. 2017, Shocket et al. 2018a, Gehman et al. 2018), and then experimentally test model predictions at the population level.

The Metabolic Theory of Ecology (MTE) is a general framework that characterizes temperature effects on physiological rates and evaluates corresponding consequences across biological levels of organization (Brown et al 2004), and which can also be used as a basis for understanding the thermal dependencies of disease traits (Rohr et al. 2011, Molnár et al. 2013a, Molnár et al 2017). MTE has been shown to capture disease-related traits such as parasite natural mortality rate (Molnár et al. 2013a), parasite equilibrium abundance within a host (Kirk et al. 2018), and host contact with parasites (Kirk et al. 2019); however, thus far, most studies linking MTE and infectious disease have operated at the individual-level. Although this framework can be scaled to predict the thermal dependence of population level properties (e.g. the basic reproductive number of the parasite  $R_0$ ; Molnár et al. 2013a), these predictions have remained untested.

An alternative approach to predicting an approaching epidemic is the theory of early warning signals (EWS) of critical transitions. EWS are statistical signatures in time series data, such as increased temporal autocorrelation and increased variability, which indicate that a critical transition is being approached (Scheffer et al. 2009). If these signals can be detected from disease incidence data before the basic reproduction number crosses the critical transition at  $R_0 = 1$ , it may be possible to forecast that an epidemic is impending without the need of a fully parameterized model. Indeed, theory and model simulations have shown that these signals can exist while a host-parasite system is slowly approaching the critical transition into an epidemic state, but are difficult to detect (O'Regan & Drake 2013). In sum, detecting EWS from incidence data or using thermal performance functions integrated within mechanistic disease models provide two approaches for predicting the emergence of an infectious disease epidemic due to warming temperatures.

Here we use the experimental host-parasite system *Daphnia magna* - *Ordoospora colligata* (a microsporidian parasite) to test if we can anticipate outbreaks of infectious disease either by using EWS or by thermally scaling model parameters in a classical susceptible-infected model for environmentally transmitted disease. The susceptible-infected model (Appendix C: Eq. 1-4) contains thirteen parameters (Table C1), six of which are temperature dependent (Kirk et al. 2018, Kirk et al. 2019a). We incorporated the thermal dependency of these parameters by fitting continuous functions of temperature using previously published MTE relationships/functions based on individually infected hosts (see Fig. C2 for MTE plots). To test if the model and/or EWS could accurately predict disease emergence in a slowly warming environment, we drove experimental host populations that experience sustained parasite immigration through slowly

warming conditions and compared the course of the resultant epidemics to constant-temperature controls. The experiment carried four host-parasite populations through a 3.5°C warming over 120 days from predicted low-disease conditions at 10°C, across the predicted  $R_0 = 1$  boundary near 12°C, and into disease invasion conditions up to 13.5°C (Fig. 9). The four control host-parasite populations were held at 10°C at which the disease was not expected to establish. We collected infection data on 516 individuals per population (12 individuals per population every 3 days over 120 days, with an additional 36 individuals on the final day) for a total of 4128 individuals from eight populations over the course of the experiment (Appendix C).

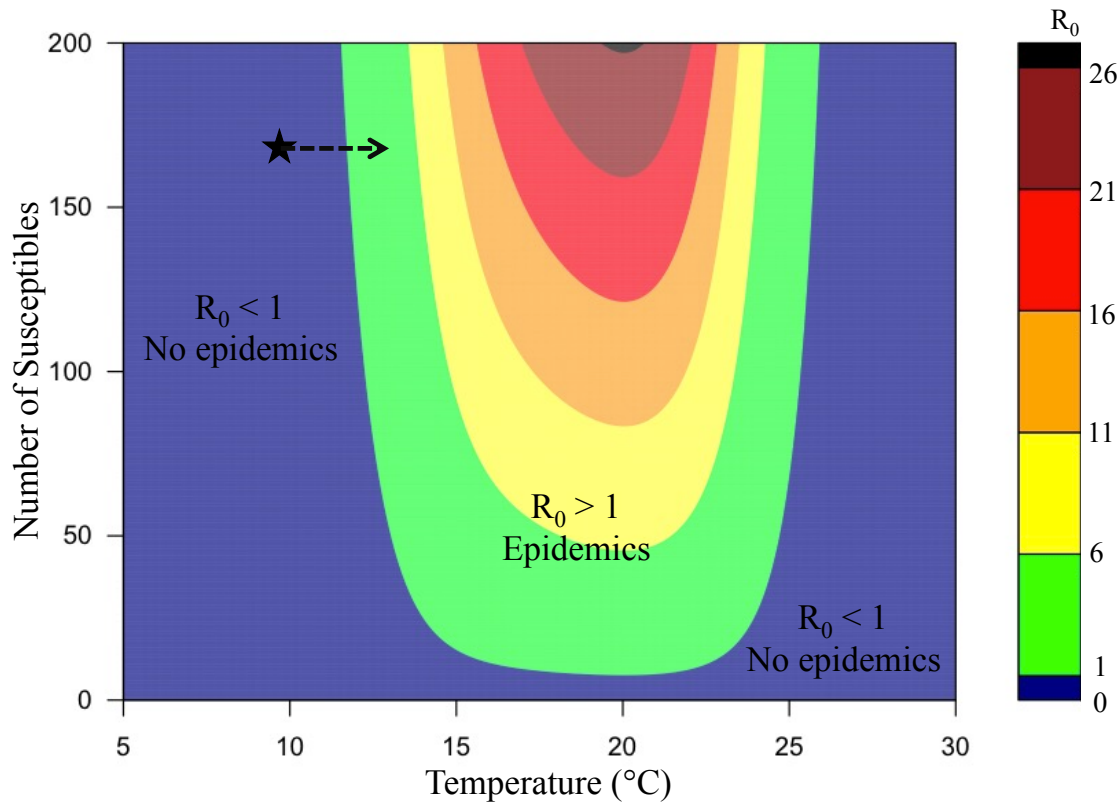


**Figure 9.** The basic reproduction number ( $R_0$ ) as a function of temperature (x-axis) and susceptible host density (y-axis). Blue represents conditions in which  $R_0 < 1$  and the disease cannot spread. The star denotes the approximate initial conditions of our experiment and the arrow denotes the trajectory of the warming populations. We did not see any clear evidence of a temperature effect on Daphnia population abundances (Fig. C1), therefore the arrow is represented as horizontal. The constant 10°C populations remained at the starred conditions for the duration of the experiment, while the warming populations moved to conditions where epidemics should occur.

Observations from experimental populations and model predictions were concordant. At very low host densities, the model predicts that the disease is unable to spread regardless of temperature (Fig. 9). At sufficiently high host density, however, temperature becomes the primary determinant of whether an epidemic can occur (Fig. 9). Early in the experiment, disease prevalence was very low across all populations (Fig. 10a,b), though the continuous but low rate of introduction of infected individuals allowed the disease to persist under unfavorable conditions (and thus be observable at a sampling frequency of once every three days). As the experiment neared its mid-point (day 60) and warming populations reached 11.5°C - 12°C, the frequency and number of infected individuals detected increased in the warming populations (Fig. 10b). This trend of increased disease prevalence continued as temperature increased in warming populations, whereas the control populations that remained at 10°C never experienced a clear increase in disease incidence (Fig. 10a). The model accurately predicted both that disease prevalence rose quickly once temperatures reached 12°C (Fig. 10a), and that the disease was maintained at less than 10% prevalence when temperatures remained constant at 10°C (Fig. 10b).

To look for early warning signals (statistical signatures) that a critical transition into an epidemic state was being approached (O'Regan & Drake 2013), we analyzed the experimental data as well as simulated data at high temporal resolution via a stochastic implementation of the model (Fig. 10c,d; Appendix C). We did not find any evidence for two key EWS - temporal autocorrelation and the coefficient of variation - in the disease incidence data from the experiment (Fig. C5-C6). Consistent with this empirical result, analysis of high-resolution simulated data indicated that the negative empirical result was not a case of sampling error or sparse data, but rather an inability of the EWS metrics variability and temporal autocorrelation to

**foreshadow the critical transition into an epidemic state in our system** (Fig. 10c,d). We note that across one thousand simulations, there was an increase in mean temporal autocorrelation preceding the critical transition which conforms to EWS theory (Fig. 10d solid red line), but this is unlikely to be detectable in practice based on the very high levels of variability in our model (Fig. 10d dashed red lines).

On the final day of the experiment we assessed an additional 36 individuals per population ( $12+36=48$  total; approx. 30% of the total population) to obtain a better indication of the true disease prevalence in the population. **We found that the warming populations (mean = 23%) had significantly higher disease prevalence ( $p = 0.027$ ; Mann-Whitney test; Fig. 11) at the conclusion of the experiment relative to the constant  $10^{\circ}\text{C}$  populations (mean = 3%).**

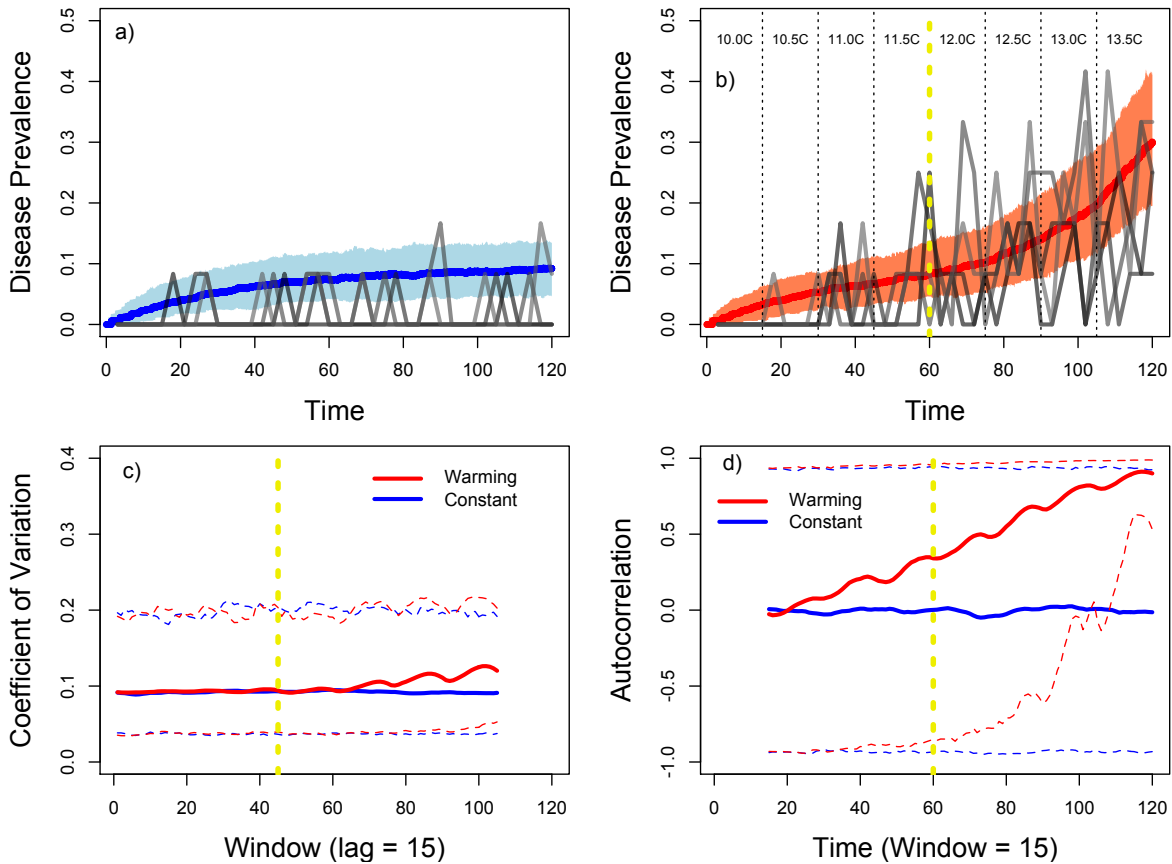


**Figure 10.** Panels a-b: Experimental data from four replicate control (constant 10.0°C) populations (a; grey lines) and four replicate warming populations (b; grey lines). Blue (a) and red (b) lines represent the median of 250 stochastic simulations of the MTE model. Light blue and light red shaded areas represent 95% confidence intervals from simulations. Note that due to the continuous input of infected individuals into the experiment, the disease is predicted to be present at low prevalence even when  $R_0 < 1$  (a; constant 10.0°C). Panels c-d: coefficient of variation (CV) (c) and temporal autocorrelation (d) for disease incidence in constant 10.0°C (blue) and warming (red) model simulations with burn-in. Solid red and blue lines represent mean CV and autocorrelation across 1000 simulations for warming and constant 10.0°C conditions respectively. Dashed red and blue lines represent 95% confidence intervals across 1000 simulations. Vertical yellow dashed line represents the temperature/time point at which the MTE model predicts  $R_0 > 1$ .

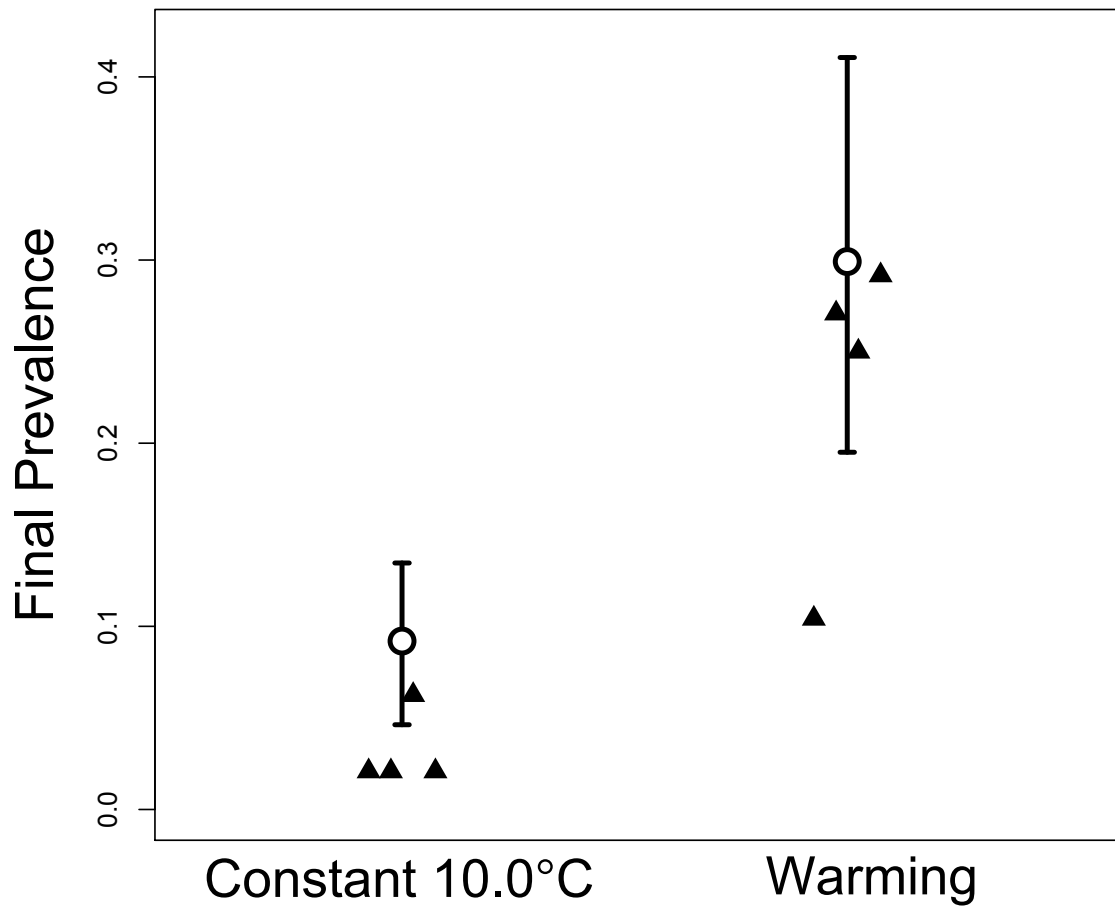


**Figure 11.** Observed final prevalences based on 48 individuals (~30% of population; solid triangles) compared to predicted final prevalences from stochastic MTE model (hollow circles). Error bars represent 95% confidence intervals on the final prevalences observed in 250 stochastic simulations.

Our experiment provides empirical evidence that slowly increasing temperatures can cause disease-free populations to cross the critical transition at  $R_0 = 1$  into an epidemic state, and that combining MTE with a mechanistic disease model enables the prediction of disease emergence in warming environments (Fig. 9-11). Because thermal response curves specified by MTE can be parameterized to a large extent by theory and meta-analyses (Molnár et al. 2017), our results open the door to the possibility that linking MTE with models of disease spread may provide a general framework for predicting climate warming effects on disease emergence across study systems and biogeographic regions while requiring less data and resources to independently parameterize models for each case.

The MTE-disease framework may also be useful for predicting range shifts of infectious disease as well as disease fade-out arising from climate warming. For example, the model predicts that if we had started the experiment near 23°C, epidemics would have initially occurred in both the constant temperature and warming treatments, and warming would have pushed those populations into disease eradication. For a given system, knowledge of host density, environmental temperature and magnitude of warming should enable one to use this modeling framework to predict whether warming should lead to epidemics or disease eradication. Whether increases in mean temperature will generally lead to more or less epidemics in general will depend on the balance between the number of host-parasite systems that will be pushed into  $R_0 > 1$  space (e.g. the star in Fig. 9) and those which will be pushed from epidemics into  $R_0 < 1$  space.

Although the model was able to accurately capture the thermal dependency of disease emergence, it did slightly overestimate disease prevalence in the constant 10°C treatment (Fig.

10-11). The observed disease prevalence in our constant 10°C populations was less than the model predicted because the MTE model likely overestimates within-host parasite equilibrium abundance at this temperature. Indeed, there is large uncertainty at which precise temperature parasite equilibrium abundance decreases to zero, although it is clear that this should occur between 9.5 and 11.8°C (Kirk et al. 2018). Beyond reducing uncertainty in MTE parameter estimates, there are additional complexities that could be incorporated into this model or models for other host-parasite systems. For example, though we did not have information to parameterize these functions here, incorporating the temperature dependence of environmental spore mortality and microparasite shedding rates by hosts could improve the quantitative match between model predictions and observed disease dynamics, but was not necessary, as the qualitative results were generally insensitive to a range of parameter values for these traits (Fig. C3; Table C2).

Our model was based on an experiment that was conducted in a climate-controlled environment; therefore, both the experimental results and the model disregard temperature fluctuations that may be important in natural systems. Daily and seasonal fluctuations, along with the predicted climate-change induced increase in temperature variability and the frequency of extreme events (Easterling 2000), remain dimensions of climate change that are yet to be explored with this MTE framework. However, methods such as nonlinear averaging may provide a promising approach to incorporating these fluctuations in performance into generalized testable predictions (Bernhardt et al. 2018a).

In addition to longer-term climatic changes in temperature, seasonal dynamics can also have large impacts on infectious disease (Altizer et al. 2006). Our results can inform the

seasonality of disease dynamics, as our slowly warming experimental system mimics the onset of spring. Indeed, many populations living in intermediate and polar climates encounter seasonal variation in temperature that far exceeds our experimental change of 3.5°C over four months. For instance, the water temperature of temperate lakes can increase from 4°C during the winter to greater than 25°C during the summer months (O'Reilly et al. 2015). In these systems, disease is typically regulated by temperature and ecological variables that are correlated with temperature (Alitzer et al 2013). Warming can alter the seasonality of epidemics either by causing epidemics to occur earlier in the season (Shocket et al. 2018a), lead to larger transmission peaks in the fall, or even split one annual transmission period into two distinct seasonal transmission periods (Molnár et al. 2013a). Determining the likelihood of these events is critical to predicting and mitigating future epidemics; utilizing mechanistic models of disease transmission with temperature-dependent parameters has been shown to be valuable in describing the seasonality of infectious disease before (Molnár et al. 2013a, Shocket et al. 2018a, 2018b, Gehman et al 2018).

Beyond causing changes in key epidemiological parameters such as contact rate, temperature may also indirectly or directly affect host population density (Myers 2001) – another key variable in determining  $R_0$ . For example, changing temperatures may alter the amount of available habitat for a population (Cline et al. 2013), indirectly leading to reduced or increased competition and larger or smaller population densities respectively. MTE suggests that increased temperatures will result in lower population carrying capacities for ectothermic hosts due to the increased per capita metabolic demands of individuals (Savage et al. 2004), though this effect may be counteracted by changes in resource availability. Here, we did not see any evidence of a temperature effect on *Daphnia* population abundances (Fig. C1), and therefore did not allow

population densities to vary with temperature in our model. However, densities will be influenced by temperature in many other systems and these changes can also be captured by MTE, for example, as demonstrated in phytoplankton (Bernhardt et al 2018b). In general, the effects of warming temperatures on host density are likely to involve both increasing and decreasing levels of disease risk, depending on the path taken by the system when transiting the density and thermal response surface (e.g. Fig. 9).

The experiment and model did not reveal early warning signals (EWS) for an epidemic as the  $R_0 = 1$  boundary was being approached (Figs. C5-C9). Since the sampling resolution of the empirical data may have been limiting, we also analyzed high resolution data from stochastic simulations of the model without sampling error (Fig. C7), a best case scenario, but did not see clear signs of EWS (Figs. C8-C9) even in this case. It is possible that we did not detect EWS because our population sizes (~170 individuals; Fig. C1) were relatively small compared to natural populations where these signals may be looked for (e.g. a human population in a large city). Indeed, O'Regan and Drake (2013) suggest that the ability to use EWS for predicting emerging epidemics will depend on the characteristics of surveillance data. Our experimental and simulation results indicate that disease emergence may not be presaged by EWS for small host populations experiencing slow environmental change, a case that may be more applicable to conservation than human health.

A predictive general framework for climate effects on infectious disease is required to advance the general debate regarding how climate change will affect disease (Altizer et al. 2013); linking MTE with host-parasite models could fill this gap (Rohr et al. 2011, Molnár et al.

2017). Accumulating evidence has shown that MTE models are able to capture the thermal dependence of many host-parasite traits (Molnár et al. 2013a, Kirk et al. 2018, Shocket et al. 2018a, Kirk et al. 2019a), and we show here that these models can be scaled up to accurately predict population level disease dynamics in a warming or constant environment. Applying this framework to host-parasite systems should provide a useful tool for predicting the effects of warming on disease epidemics.

## Appendix C

### Chapter 3

#### Materials and Methods

##### *Host-parasite system*

*Ordospora colligata* is an environmentally-transmitted microsporidian parasite of *Daphnia magna*, a small freshwater invertebrate. The parasite infects the epithelial cells of its host's gut after being inadvertently ingested by the host during filter feeding (Ebert 2005). The parasite replicates intracellularly, eventually lysing the cell and releasing spores that spread to nearby gut cells or are released into the water column where they can go on to infect other individuals. All *Daphnia* individuals in this experiment (and in the previous experiments used to parameterize our model) are from one Finnish clone (FI-OER-3-3), from which the parasite strain (OC3) used here was originally isolated.

##### *Experimental Methods*

The experiment was initiated with eight 35L tanks that housed populations of uninfected *Daphnia*. Prior to the experiment, these populations were maintained at lab conditions (20°C) for fifteen days before they were moved into four environmental growth chambers set to 10°C. They remained at 10°C for another fifteen days to allow for acclimatization, and population abundances stabilized between 150 and 240 large (approximately 2.7mm in length) individuals before the experiment began (Fig. C10). On day zero of the experiment we introduced three large individuals that had been exposed to the parasite into each of the eight experimental populations. The twenty-four introduced animals were randomly selected from stock cultures, kept in multiple

2L mesocosms, that were exposed to the parasite for ~12 months prior to and throughout the experiment. Prevalence in these mesocosms was determined near the mid-point of the experiment by randomly selecting 314 individuals across all stocks and was found to be 46.50% (i.e. on average we introduced 1.4 infected animals into each experimental population). These exposed stock cultures were maintained at 20°C, meaning that the individuals introduced from these populations were not acclimatized to 10°C. We did this to ensure that infections successfully established, rather than risk that animals lost their infection prior to introduction into the experimental populations as infectivity is low at 10°C and infections have rarely been reported at this temperature (Kirk et al. 2018, 2019). An additional experiment revealed no signs of increased mortality in the first 24h after a group of 20 individuals was transferred from 20°C to 10°C (animals alive after the temperature shift:  $19.6 \pm 0.6$ , animals alive in the control:  $19.3 \pm 0.6$ , 3 replicates per treatment). We note that other rates such as filtration may not be immediately acclimatized to 10°C, though the acclimatization process for this is generally quite rapid (Kirk et al. 2019).

On day three and every three days for the duration of the experiment, we randomly sampled twelve large individuals from each population. Large individuals were chosen to increase the probability that potential infections could be detected within the individuals, as it is difficult to detect *O. colligata* infections in small *D. magna*. These individuals were inspected under phase contrast microscopy to assess, 1) whether they were infected and, 2) infection load. We then introduced three individuals from our infected stocks as described above for day zero. Since our sampling and microscopy process is destructive, we also introduced nine large uninfected *Daphnia* individuals that were acclimatized from 20°C to their new temperature for fifteen days. These animals were randomly selected from stock cultures that were not exposed to

the parasite (kept under identical conditions as described above for the exposed stocks). In sum, every three days we removed twelve individuals and introduced twelve new individuals. Of these twelve new individuals, on average 1.4 were infected (i.e. three individuals from infected stocks \* 0.465 infection prevalence in these stocks), with a minimum of zero and a maximum of three infected. Each sampling day we also removed 3L of medium Aachener Daphnien Medium (ADaM using only 5% of the recommended SeO<sub>2</sub> concentration, Klüttgen 1994) and replaced it with 3L of new ADaM. Assuming that *Ordospora* spores are evenly distributed throughout the medium, our experimental process of removing 3L of the 35L every three days invoked a mortality rate of 0.0286 d<sup>-1</sup>. Finally, each population was fed 350 million batch cultured algae (*Monoraphidium minutum*) each sampling day.

After fifteen days (i.e. five sampling days), we raised the temperature in two of the environmental growth chambers (i.e. experimental populations 5 – 8) by 0.5°C to 10.5°C while the other two chambers remained at 10°C. This process continued for a total of 120 days, resulting in 40 sampling days (480 samples per population). At the conclusion of the experiment, 15 days after the last temperature increase to 13.5°C, we sampled an additional 36 individuals per population (for a total of 48 individuals per population on day 120) to provide a better estimate of disease prevalence.

On days 0, 15, 30, 45, 60, 75, 90, 105, and 120 we conducted population size estimates via visual inspection. In each population, we estimated the number of large *D. magna* (i.e. individuals large enough to be considered for random sampling of infection status on sampling days). We repeated each population estimate three times to obtain an estimate of our variation in counts. We note that each experimental population also included numerous juvenile *D. magna*, but we did not include them in abundance counts as we would not have sampled them for

infection status. Additionally, larger (and therefore older) *D. magna* will have had significantly more time for the infection to progress within them (Kirk et al. 2018), and therefore contribute significantly more to the force of infection in the population.

Although at times, especially earlier in the experiment, there was large variation between populations, we did not observe any clear differences in population abundances in warming versus constant 10°C experimental populations (Fig. C1). This suggests that differences in population size was not the driver of higher disease prevalence in the warming treatments versus in the constant 10°C treatments. Moreover, population sizes seemed to decrease slightly over the earlier portion of the experiment before approximately levelling out at approximately 150 individuals at the conclusion of the experiment, again suggesting that differences in abundance can not explain the increase in the warming populations. The mean population size across all populations throughout the experiment was 169.48, therefore we set the density-dependent constraint on recruitment (K) to be 170 in our epidemiological model.

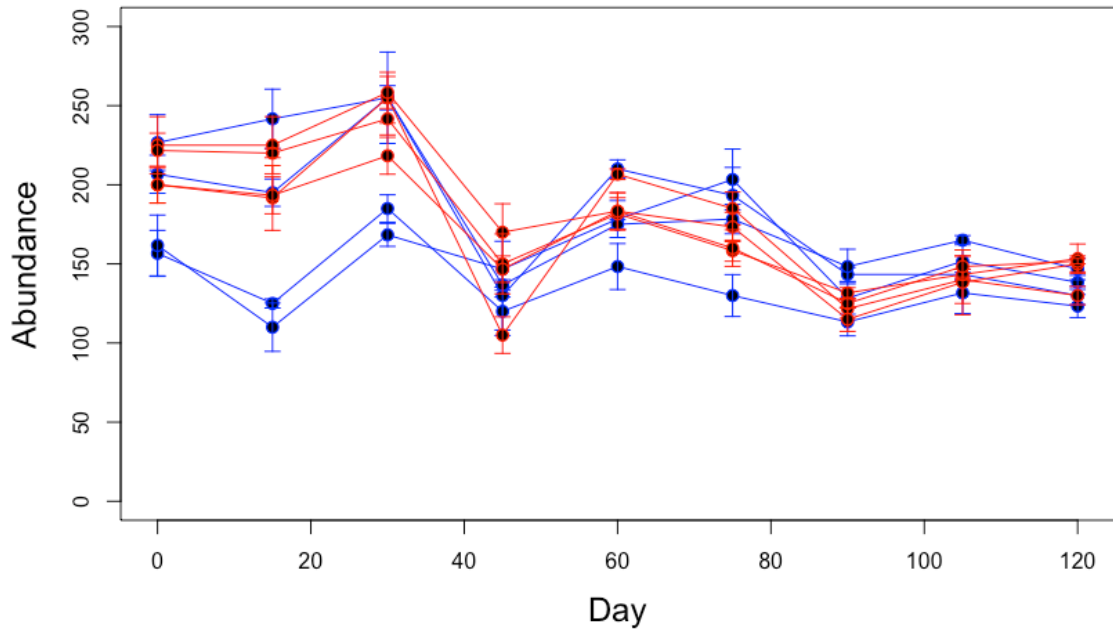


Fig. C1. *Daphnia magna* abundances in experimental populations. Blue and red points and lines represent populations in constant 10.0°C and warming conditions respectively. Points represent the mean of three counts for each population, and error bars represent the maximum and minimum value from these three counts.

### Model

We adapted a susceptible-infected disease model to track susceptible hosts (S; Eq. C1), infected hosts (I; Eq. C2), dead infected hosts that can still shed the parasite (D; Eq. C3), and environmental spores (E; Eq. C4).

$\frac{dS}{dt} = \phi_S + \psi(S + I)\left(1 - \left(\frac{S + I}{K}\right)\right) - \chi(T)\sigma(T)SE - \mu(T)S - h(S + I)\left(\frac{S}{S + I}\right)$	Eq. C1
$\frac{dI}{dt} = \phi_I + \chi(T)\sigma(T)SE - (\mu(T) + \alpha(T))I - h(S + I)\left(\frac{I}{S + I}\right)$	Eq. C2
$\frac{dD}{dt} = (\mu(T) + \alpha(T))I - \theta D$	Eq. C3
$\frac{dE}{dt} = \lambda(T)I + \omega(T)\theta D - \gamma E$	Eq. C4

This model can then be used to generate an expression for the basic reproductive number  $R_0$  (Eq. C5):

$$R_0(T) = \left( \frac{\lambda(T)}{\mu(T) + \alpha(T) + h} + \omega(T) \right) \left( \frac{\chi(T)\sigma(T)S_{eq}}{\gamma} \right) \quad \text{Eq. C5}$$

where  $\lambda(T)$  is parasite shedding from the host,  $\mu(T)$  is natural host mortality,  $\alpha(T)$  is parasite-induced mortality,  $h$  is harvesting mortality,  $\omega(T)$  is the number of spores released at host death,  $\chi(T)$  is contact rate,  $\sigma(T)$  is probability of infection after contact,  $S_{eq}$  is susceptible host density, and  $\gamma$  is parasite spore mortality. Here,  $(T)$  denotes that a parameter is a function of temperature. The parameterized model predicts the conditions for host density and thermal conditions under which the disease cannot invade ( $R_0 < 1$ ) versus epidemic conditions ( $R_0 > 1$ ) (Fig. 9).

In Eq. C1 - C4, susceptible individuals are added to replicate populations via our experimental protocol (see experimental methods) ( $\phi_S$ ) or by natural density-dependent recruitment, and are lost via natural mortality ( $\mu$ ), by being harvested out of the experiment ( $h$ ) or by becoming infected at a rate of  $\chi\sigma SE$ . The product of contact rate ( $\chi$ ) and the probability of infection after contact ( $\sigma$ ) is the transmission coefficient that is classically represented by the parameter  $\beta$ , but separated here to allow for modeling via MTE (Kirk et al. 2019). Infected individuals are added via transmission or by addition of infected animals from source populations ( $\phi_I$ ). Conversely, they are lost via natural mortality and added parasite-induced mortality ( $\mu + \alpha$ ) as well as by being harvested out of the experiment ( $h$ ). Infected individuals that die transition to the  $D$  class and are eventually lost via degradation ( $\theta$ ). Environmental spores are released into the environment via continuous shedding by infected individuals ( $\lambda$ ). Spores are

also released from dead infected individuals at rate  $\omega\theta$ , where  $\omega$  is the number of spores in the host when they die. Here, we assume that all spores from the dead infected host are eventually released; therefore the rate is the product of the number of spores in the host ( $\omega$ ) and the degradation rate ( $\theta$ ). In other words, degradation rate ( $\theta$ ) is included to fine-tune the number of parasite spores released from a dead infected host per time step.

Parameters in the model were either modeled as continuous functions of temperature or did not vary with temperature (Table C1). The Van't Hoff-Arrhenius equation, in which the rate of a process depends on the activation energy, the Boltzmann's constant and the temperature, has been frequently used to capture thermal scaling relationships (Brown et al. 2004). However, since high or low temperatures can impede biological processes due to the inactivation of enzymes, this relationship can be modified to incorporate temperature thresholds leading to the Sharpe-Schoolfield equation and its variants (Schoolfield et al. 1981; Molnár et al. 2017; Kirk et al. 2018). Our previous work has shown that these metabolic models can accurately capture the thermal dependencies of the host-parasite processes in the *Daphnia-Ordospora* model system (Kirk et al. 2018, Kirk et al. 2019). We used these previously published MTE functions to capture the parameters in Eq. C1-C4 that were temperature-dependent (see Table C1) and thus these parameterizations are independent from our experiment.

Table C1. Parameters for Eq. 1-5 in Chapter 3.

Temperature-Independent Parameters			
Parameter	Description	Source	Value
$\phi_S$	Input of susceptibles	Methods used in this study	3.535 d <sup>-1</sup>
$\phi_I$	Input of infecteds	Methods used in this study	0.465 d <sup>-1</sup>
$K$	Density-dependent recruitment constraint	Abundance measured in this study	170
$\varphi$	Per-capita recruitment	Experimental abundances	1.33 d <sup>-1</sup>
$h$	Harvesting	Methods used in this study	0.0235 d <sup>-1</sup>
$\gamma$	Environmental spore mortality	Experimental medium removal rate used in this study	0.0286 d <sup>-1</sup>
$\theta$	Corpse degradation	Average from degradation experiment	0.1 d <sup>-1</sup>

Temperature-Dependent Parameters			
Parameter	Description	Source	Function
$\mu(T)$	Natural mortality rate	Kirk et al. 2018. PLoS Biology.	Sharpe-Schoolfield <sup>1+</sup>
$\chi(T)$	Contact rate	Kirk et al. 2019. The American Naturalist.	Sharpe-Schoolfield <sup>1</sup>
$\sigma(T)$	Probability of infection	Kirk et al. 2019. The American Naturalist.	Sharpe-Schoolfield* <sup>1</sup>
$\lambda(T)$	Parasite shedding rate	Kirk et al. 2018. PLoS Biology.	Sharpe-Schoolfield <sup>o1</sup>
$\alpha(T)$	Parasite virulence rate	Kirk et al. 2018. PLoS Biology.	Sharpe-Schoolfield <sup>o1</sup>
$\omega(T)$	Parasite load at host death	Kirk et al. 2018. PLoS Biology.	Sharpe-Schoolfield <sup>o1</sup>

<sup>1</sup> See Fig. C2 for functional forms.

+ Natural mortality rate arises from a Weibull survival model in which the scale parameter is modeled with an inverse Sharpe-Schoolfield and the shape parameter is modeled with a Sharpe-Schoolfield.

\* Probability of infection arises from modeling infection rate using Sharpe-Schoolfield and gut residence time using Sharpe-Schoolfield and Daphnia body size.

<sup>o</sup> Parasite shedding rate, per-parasite virulence, and parasite load at death are all modeled as functions of the same within-host parasite abundance. Within-host parasite-abundance is modeled using the Sharpe-Schoolfield.

### Disease model parameterization and assumptions

Seven parameters were modeled as temperature independent. The input rate of susceptibles ( $\phi_S$ ) and infecteds ( $\phi_I$ ) was determined by experimental conditions and the prevalence of infections in the stocks from which exposed individuals were introduced into the experiment ( $\phi_S = 3.535 \text{ d}^{-1}$ ,  $\phi_I = 0.465 \text{ d}^{-1}$ ). Twelve of the ~170 individuals were harvested every three days; therefore, harvesting rate ( $h$ ) was set to  $0.0235 \text{ d}^{-1}$ . Environmental spore mortality was set to equal the rate at which we removed medium (3 of the 35L / 3 days):  $\gamma = 0.0286 \text{ d}^{-1}$ . Infected corpse degradation rate, which does not affect  $R_0$  but affects the timing of how quickly spores are released into the environment, was set to  $0.1 \text{ d}^{-1}$ . This is the average degradation rate in an independent experiment we conducted where we visually assessed the time point at which the *Daphnia* gut was approximately completely degraded. We note that this value ( $0.1 \text{ d}^{-1}$ ) was averaged across nine experimental temperatures ( $5^\circ\text{C} - 32^\circ\text{C}$ ), and while degradation did increase with temperature, we did not use MTE to model it as the parameter does not appear in the  $R_0$  equation (Eq. C5) and therefore does not affect the critical transition temperature to an epidemic.

Maximum recruitment rate ( $\psi$ ) was set to 1.33 to allow for population abundances to remain around the carrying capacity  $K$ , which was set to 170 to mirror the approximate abundances in the experiment (Fig. C1). Finally, since we did not measure *Daphnia* length in the experimental populations, we estimated a length of 2.7mm for the large individuals that were sampled based on previous observations of our stock populations. We explored the effects of this assumption using further simulations and did not observe any large changes in model predictions (Fig. C3).

To capture parameters that scaled with temperature we used five different parameterizations of MTE functions. Contact rate ( $\chi$ ) was modeled using a Sharpe-Schoolfield function with only an upper temperature threshold (Kirk et al. 2019, Fig. C1), and is standardized

to the volume of the container (35L) with *Daphnia* size set to 2700 $\mu\text{m}$ . The probability of infection after contact ( $\sigma$ ) arises from a Sharpe-Schoolfield model with upper and lower temperature thresholds that predicts the infection rate within the host, as well as how long the parasite remains in contact with the host (residence time of the parasite in the gut), which in turn is determined by *Daphnia* filtration rate (i.e.  $\chi$ ) and the size of the *Daphnia* (Kirk et al. 2019, Fig. C2). Previously, we modeled natural mortality using a two-parameter Weibull distribution in which the hazard can change through time depending on the shape parameter (Kirk et al. 2018). Since we did not track individuals through time in this model, we here used a constant hazard rate ( $\mu$ ). To obtain this value for each temperature, we simulated our MTE Weibull model, using Sharpe-Schoolfield functions for both parameters, to predict the natural survival curve for an uninfected individual at each temperature. From this curve, we found the time point at which survival probability is 0.5 (i.e. the median survival) and used this as the expected lifespan. Finally, we set natural mortality rate ( $\mu$ ) in our model to be 1 / predicted lifespan.

We also used the Sharpe-Schoolfield function to model equilibrium parasite abundance within the host, which rises quickly from zero to  $\sim$ 160 parasite clusters near 10°C, and then slowly decreases as temperature increases before approaching zero clusters near 30°C (Kirk et al. 2018, Fig. C2). Since equilibrium abundance of the parasite can take months to approach in the 10 - 13.5°C temperature range (Kirk et al. 2018), we modeled infection load in our experiment as a proportion of the equilibrium abundance. We used observed infection loads from our experiment to find the average proportion of equilibrium abundance in this temperature range: 0.182. This infection load temperature function was then used to predict the parasite-induced mortality rate ( $\alpha$ ), parasite shedding rate ( $\lambda$ ) and the number of spores in the host when it dies ( $\omega$ ) for each temperature. Parasite-induced mortality rate ( $\alpha$ ) was set to the product of infection

load and  $5.12 \times 10^{-6}$ , the per-parasite added mortality previously estimated (Kirk et al. 2018). We note that because we did not track individuals through time, per-parasite added mortality is constant for an infected individual and cannot change through time, though it can change with the shape parameter in Kirk et al. 2018. For  $\lambda$  and  $\omega$ , which both relate to parasite spores rather than parasite clusters, we assume that a spore cluster has twenty-four spores, which is generally the average which we observe in the lab (between 16 and 32 spores per clusters). For  $\lambda$ , we assumed that when a parasite cluster bursts, half of the twenty-four spores are released into the environment while the other twelve remain in the host (to either re-infect or die), and that this bursting process occurs every seven days. We note that Refardt and Ebert (2006) estimate that the parasite may burst approximately every three days at room temperature, but we assume here that this takes significantly longer in our  $10 - 13.5^{\circ}\text{C}$  range since within-host parasite growth rate is depressed (Kirk et al. 2018). We refer readers to Chapter 3 for implications of modeling these rates as functions of temperature.

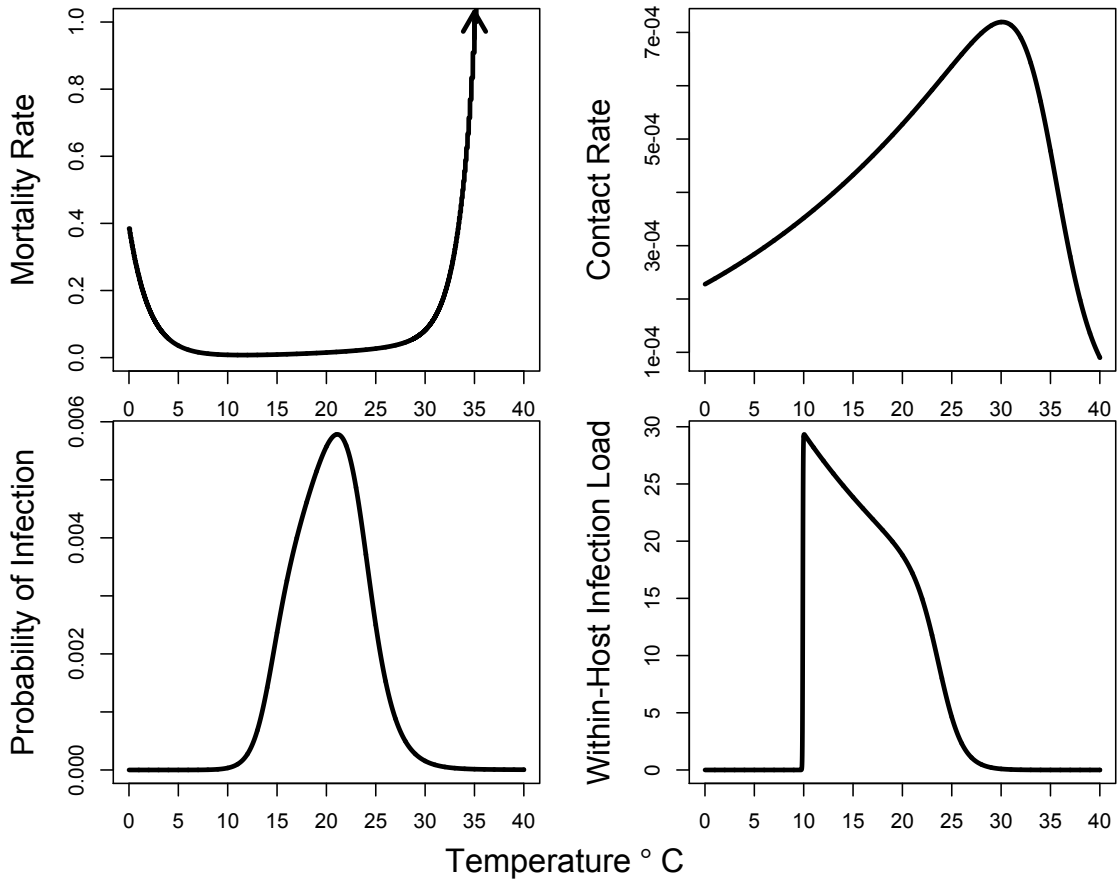


Fig. C2. Functions for mortality rate, contact rate, probability of infection, and within-host infection load.

#### *Model sensitivity to assumptions*

We explored how sensitive our model results are to five different assumptions: 1) infection load proportion of equilibrium abundance, 2) *Daphnia* size, 3) spores per cluster, 4) cluster burst time, and 5) the number of spores released out of the host per cluster. Assumptions were tested by simulating our model 250 times (without stochasticity) in which we allowed parameters to take a value from along uniform distributions (with replacement) in which the median is the value used for the main analysis, and upper and lower range limits are our best estimates at realistic ranges

for the parameter values (see Table C2). While changing the assumptions incorporated more variation, our results were generally robust across the entire parameter space (Fig. C3).

We also investigated the effects of sampling noise on our results, as we sampled a subset of the population (twelve individuals) on each sampling day. We simulated the model in a deterministic framework 250 times, and then used a binomial sampling process to randomly select twelve individuals every three days. This process captures the sampling noise observed in the warming samples well, but somewhat overestimates the sampled prevalence in the constant 10°C populations (Fig. C4).

Table C2. Range of values used in simulations to test model sensitivity to assumptions.

	Lower range limit	<b>Chapter 3</b> <b>value</b>	Upper range limit
Parasite load as proportion of equilibrium parasite abundance	0.132	<b>0.182</b>	0.232
Parasite cluster burst time	4.5	7	9.5
Spores per cluster	16	<b>24</b>	32
Proportion of spores released into environment per cluster	0.25	<b>0.50</b>	0.75
Daphnia size	2500	<b>2700</b>	2900

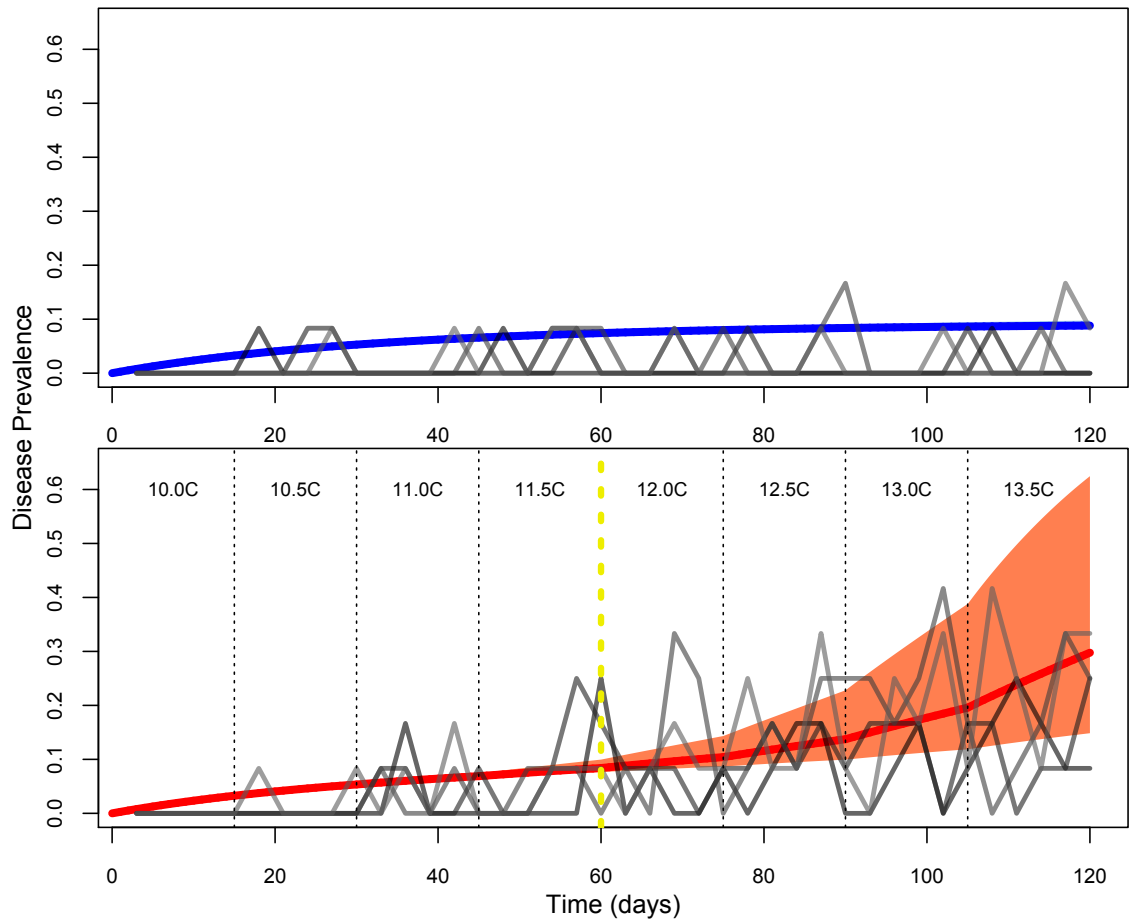


Fig. C3. Sensitivity to model assumptions. Blue (top panel) and red lines (bottom panel) represent mean disease prevalence for constant 10.0°C and warming conditions, respectively, across 250 simulations that sample from the parameter space. The shaded blue region in the top panel represents the 95% confidence interval, but is not visible due to the parameter assumptions having negligible effects on disease prevalence at 10°C. The shaded red region in the bottom panel represents the 95% confidence interval under warming conditions. The yellow, dashed vertical line represents the temperature/time point at which the MTE model predicts  $R_0 > 1$  for warming conditions.

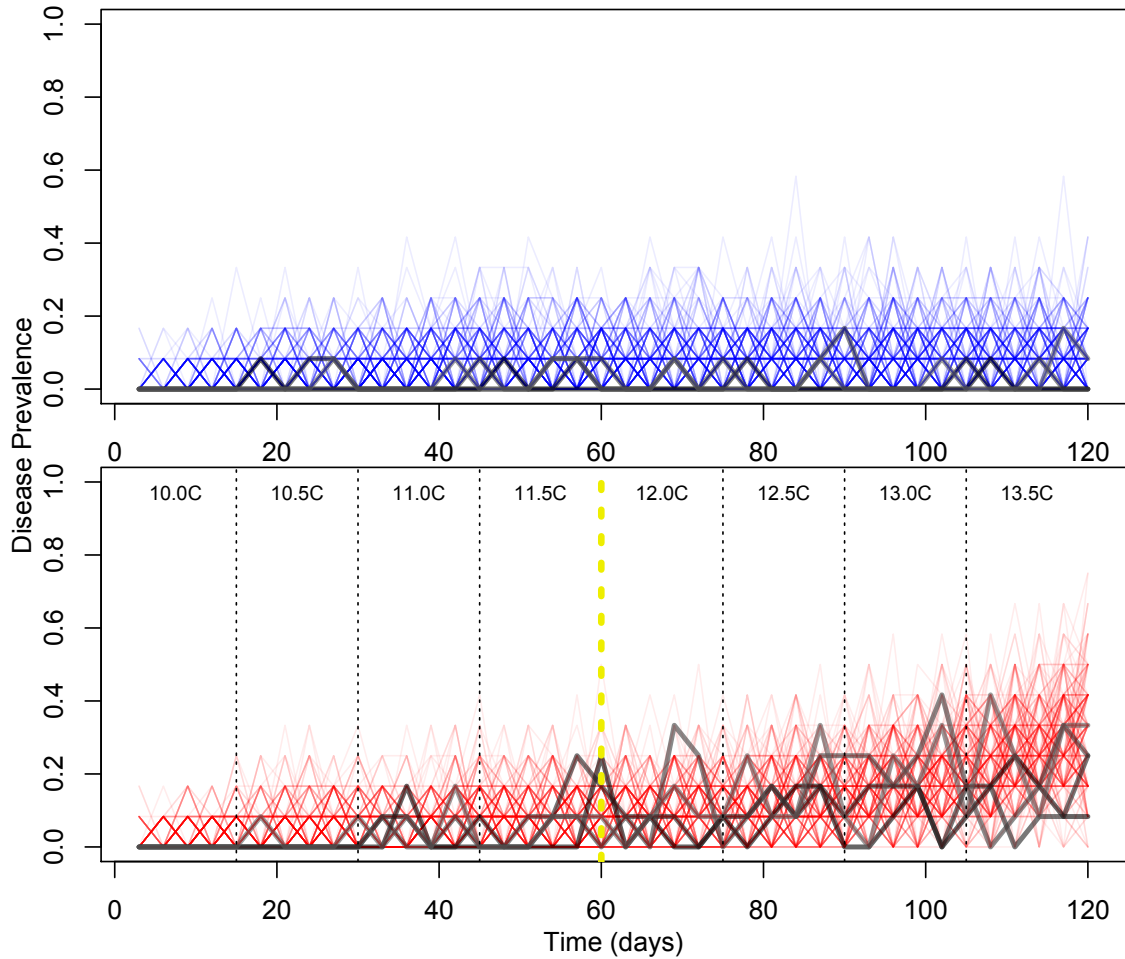


Figure C4. Effects of sampling noise. Blue and red lines represent 250 random samples from deterministic simulation of the model. Grey lines represent experimental data for constant 10°C (top panel) and warming populations (bottom panel) respectively.

## Early Warning Signals

We investigated our experimental data and simulated model for two key early warning signals (EWS) of an approaching critical bifurcation: increased coefficient of variation (CV) and increased temporal autocorrelation (AC). We refer readers to O'Regan & Drake (2013) for an in-depth discussion of early warning signals and disease emergence. We found no evidence of EWS from the experimental data (Figs. C5-C6) or from higher resolution model simulations (Figs. C8-C9).

### *Experimental Data*

For the experimental data, we investigated CV and autocorrelation across a lag/sliding window of 15 days, as this was the length of time for each temperature exposure in the warming treatment. The total experiment lasted 120 days. Disease incidence is based on samples of twelve individuals that are obtained every three days. The warming data showed no evidence of increased CV (Fig. C5) or increased autocorrelation (Fig. C6) as  $R_0 = 1$  is being approached.

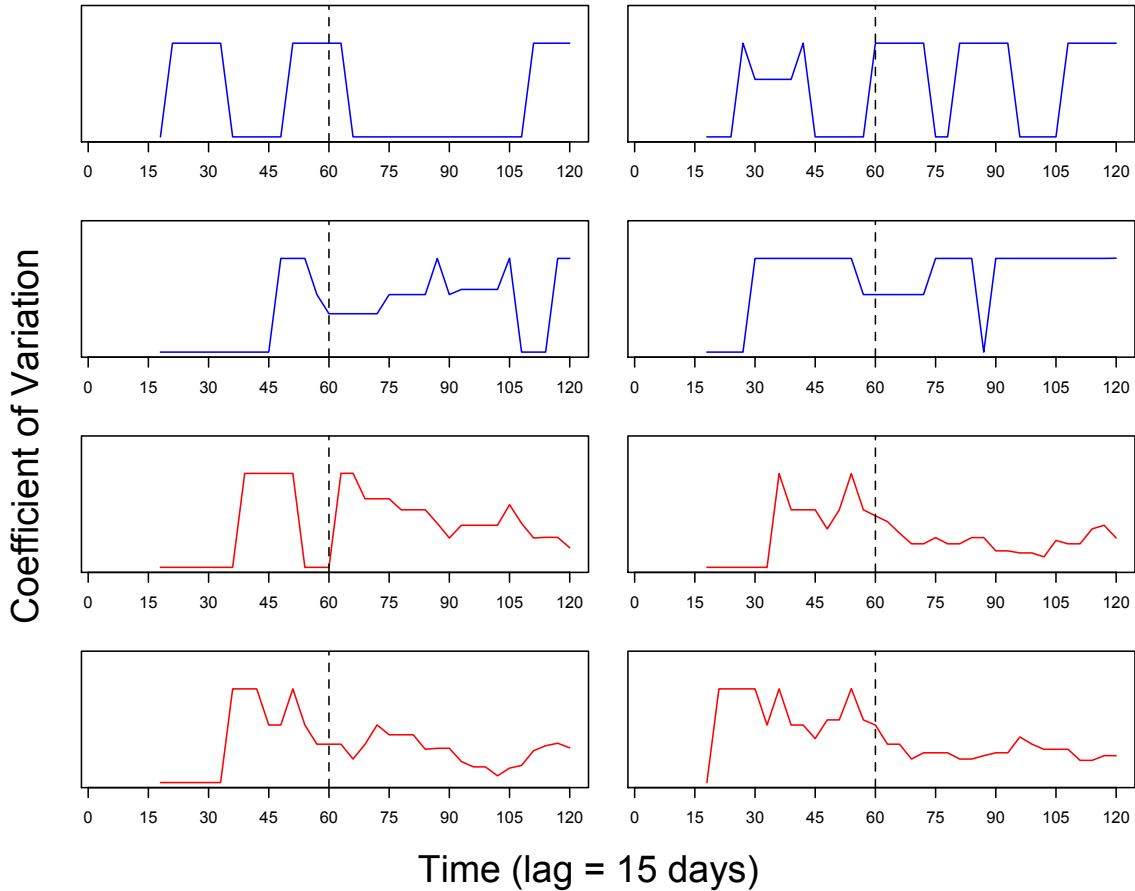


Fig. C5. Coefficient of variation for disease incidence in constant 10.0°C (blue) and warming (red) experimental populations. The black, dashed vertical line represents the temperature/time point at which the MTE model predicts  $R_0 > 1$  for warming conditions.

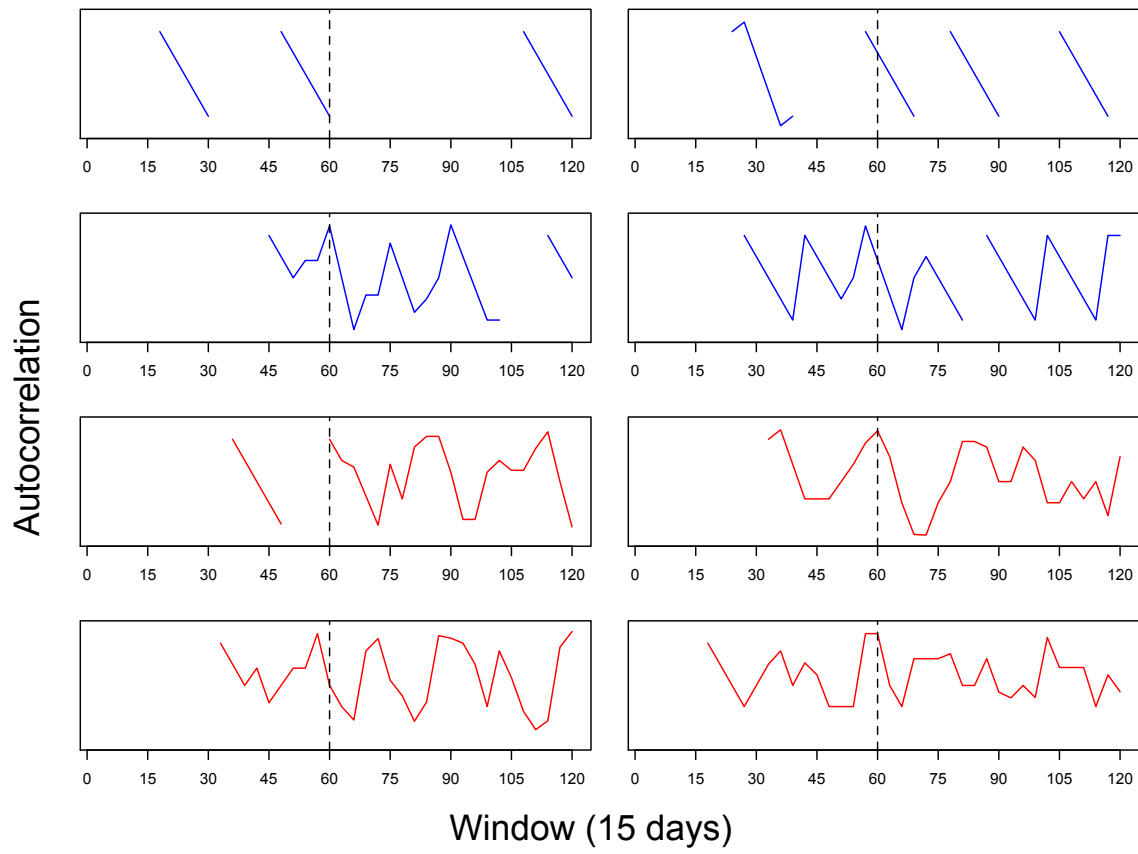


Fig. C6. Autocorrelation for disease incidence in constant  $10.0^{\circ}\text{C}$  (blue) and warming (red) experimental populations. Gaps are caused when incidence does not change across the window. The black, dashed vertical line represents the temperature/time point at which the MTE model predicts  $R_0 > 1$  for warming conditions.

### *Model*

We simulated our constant temperature and warming temperature MTE-based model one thousand times each in a stochastic framework using the Gillespie method in R (GillespieSSA package). We allowed our model to burn-in for 365 days at  $10.0^{\circ}\text{C}$  conditions so that disease prevalence was at a steady state. The constant  $10.0^{\circ}\text{C}$  simulations then continued at the same conditions for an additional 105 days (470 days total), while the warming simulations were raised  $0.5^{\circ}\text{C}$  every 15 days starting on day 365 until completing fifteen days at  $13.5^{\circ}\text{C}$  on day

470 (Fig. C7). We looked at CV and AC across three lengths of lag/sliding windows: 5, 15, and 30 days (Figs. C8-C9). Disease incidence is the true number of infected individuals in the entire populations and is calculated daily. Comparing 95% confidence intervals in Figs. S8-S9 reveals that there is no evidence of increasing CV or AC in the warming treatment compared to the 10.0°C before the critical transition. There were increases in mean temporal autocorrelation preceding the critical transition which conforms to EWS theory (Fig. C9 solid red lines). However, very high levels of variability and confidence intervals that span almost the entire -1 to +1 autocorrelation space (Fig. C9 dashed red lines) suggest that this metric would not be usable in practice here.

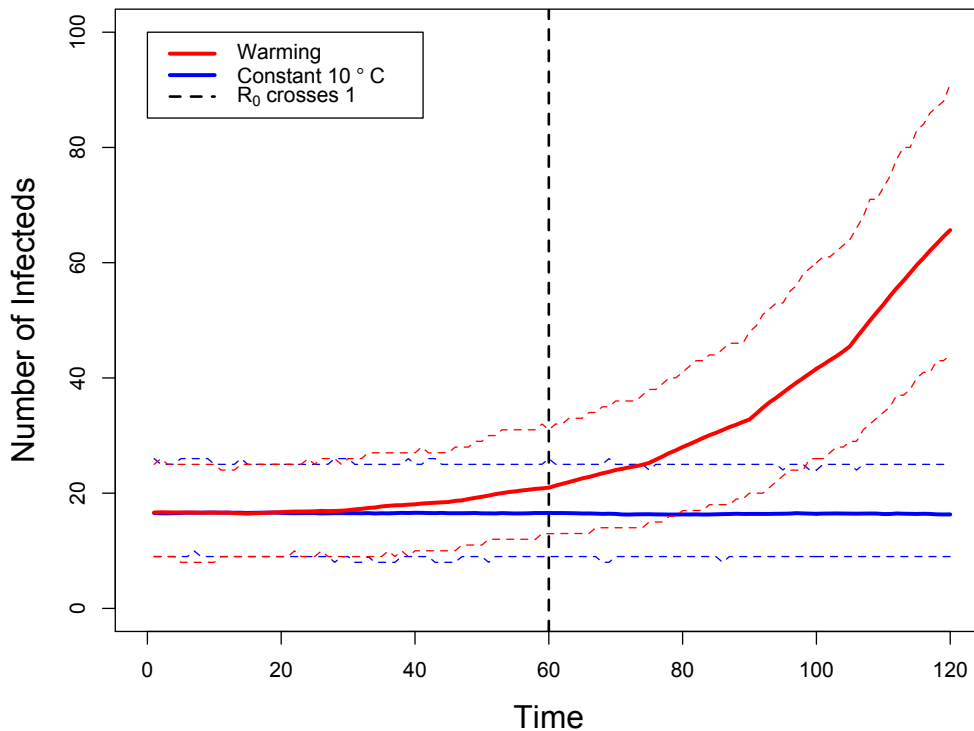


Fig. C7. Number of infected individuals in model simulations with burn-in. Solid red and blue lines represent mean number of infecteds across 1000 simulations for warming and constant 10.0°C conditions respectively. Dashed red and blue lines represent 95% confidence intervals across 1000 simulations. The black, dashed vertical line represents the temperature/time point at which the MTE model predicts  $R_0 > 1$  for warming conditions.

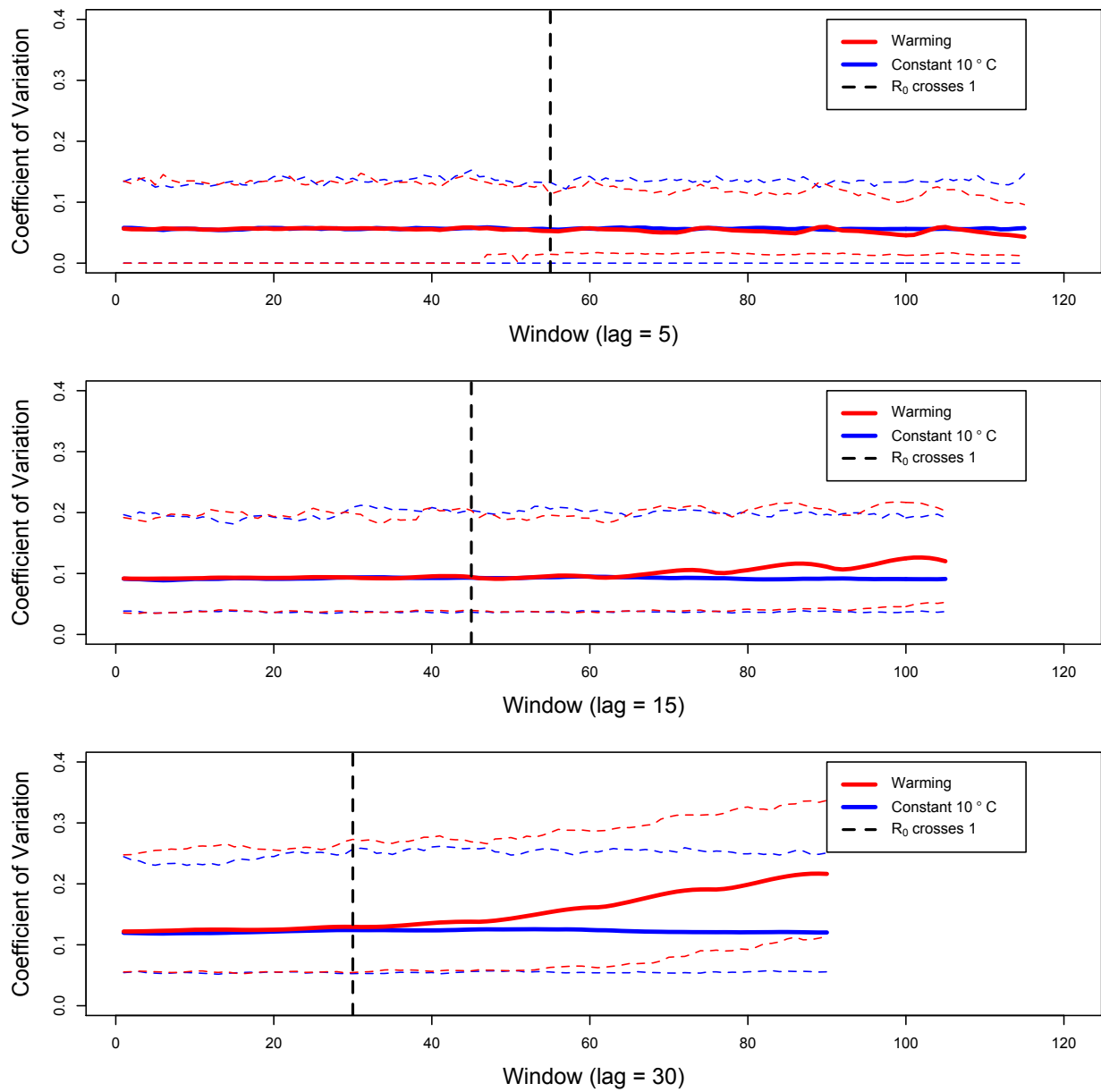


Fig. C8. Coefficient of variation for disease incidence in constant 10.0°C (blue) and warming (red) model simulations with burn-in with lag of 5, 15, and 30 days. Solid red and blue lines represent mean coefficient of variation across 1000 simulations for warming and constant 10.0°C conditions respectively. Dashed red and blue lines represent 95% confidence intervals across 1000 simulations. The black, dashed vertical line represents the temperature/time point at which the MTE model predicts  $R_0 > 1$  for warming conditions; therefore if EWS are present they should be evident before this region.

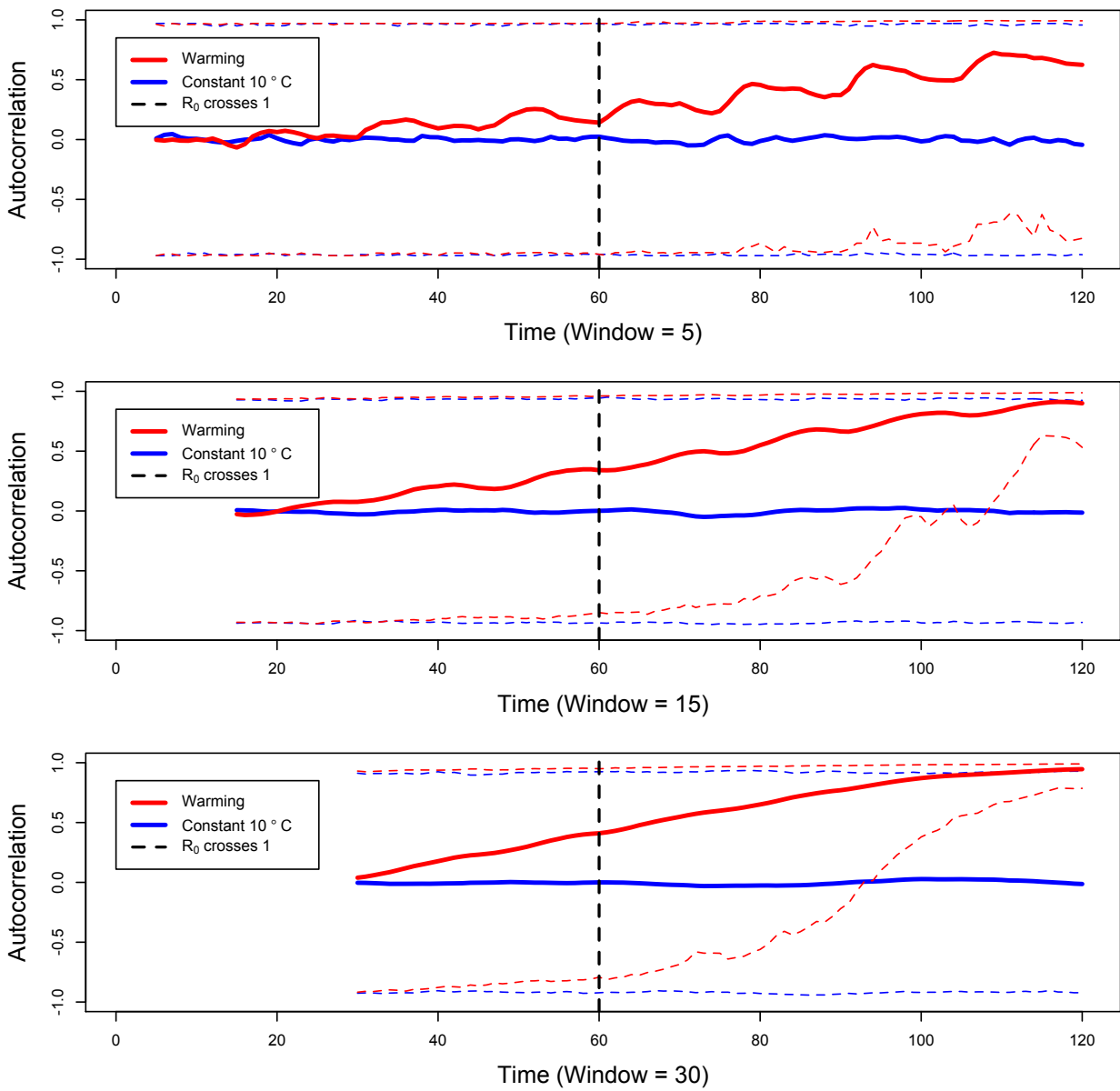


Fig. C9. Temporal autocorrelation for disease incidence in constant 10.0°C (blue) and warming (red) model simulations with burn-in with window size of 5, 15, and 30 days. Solid red and blue lines represent mean autocorrelation across 1000 simulations for warming and constant 10.0°C conditions respectively. Dashed red and blue lines represent 95% confidence intervals across 1000 simulations. The black, dashed vertical line represents the temperature/time point at which the MTE model predicts  $R_0 > 1$  for warming conditions; therefore if EWS are present they should be evident before this region.